1992

The Self-Discharge of the NiOOH/Ni(OH)2 Electrode Constant Potential Study

Z. Mao
Texas A & M University - College Station

Ralph E. White
University of South Carolina - Columbia, white@cec.sc.edu

Publication Info

Journal of the Electrochemical Society, 1992, pages 1282-1289.

DOI: 10.1149/1.2069397
http://dx.doi.org/10.1149/1.2069397

the absence of oxygen (8). The electron transfer rate and diffusion coefficient of Co^{2+} ions are both decreased with the inhibiting effect of the $Co(OH)_2$ colloid layer at the vicinity of the electrode surface, as compared to that without the inhibiting effect of $Co(OH)_2$ colloid layer.

Acknowledgments

One of the authors (C.Q.C.) was in receipt of a Sino-British Friendship Fellowship and a Chinese Government Education Commission Scholarship.

Manuscript submitted Feb. 15, 1991; revised manuscript received May 28, 1991.

REFERENCES

1. A. C. C. Tseung, S. P. Jiang, Y. Z. Chen, and J. K. You, *J. Mater. Sci. Letters*, **9**, 1294 (1990).
2. S. P. Jiang, Y. Z. Chen, J. K. You, T. X. Chen, and A. C. C. Tseung, *This Journal*, **137**, 3374 (1990).
3. S. P. Jiang and A. C. C. Tseung, *ibid.*, **137**, 3381 (1990).
4. S. P. Jiang and A. C. C. Tseung, *ibid.*, **137**, 3387 (1990).
5. S. P. Jiang, C. Q. Cui, and A. C. C. Tseung, *ibid.*, Accepted.
6. C. Q. Cui, S. P. Jiang, and A. C. C. Tseung, *ibid.*, Accepted (1991).
7. L. V. Pyatnitskii, "Analytical Chemistry of Cobalt," p. 5, Israel Program for Scientific Translations, Jerusalem (1966).
8. C. Q. Cui, S. P. Jiang, and A. C. C. Tseung, *This Journal*, **137**, 3418 (1990).
9. A. J. Bard and L. R. Faulkner, "Electrochemical Methods, Fundamentals and Applications," Chap. 6, John Wiley & Sons, New York (1980).
10. S. Fletcher, *J. Electroanal. Chem.*, **118**, 419 (1981).

The Self-Discharge of the $NiOOH/Ni(OH)_2$ Electrode Constant Potential Study

Z. Mao* and R. E. White*

Center for Electrochemical Engineering, Department of Chemical Engineering, Texas A&M University, College Station, Texas 77843

ABSTRACT

Hydrogen oxidation currents at a $NiOOH/Ni(OH)_2$ electrode were measured directly at constant potentials for various hydrogen pressures and states of charge. It was found that the hydrogen oxidation current is linearly proportional to the hydrogen pressure at all electrode potentials and that the logarithm of the anodic current is a linear function of electrode potential. It was also found that hydrogen oxidation on the nickel substrate material was strongly inhibited by the presence of nickel hydroxide on the substrate surface. By comparing the currents for hydrogen oxidation and oxygen evolution on the $NiOOH/Ni(OH)_2$ electrode and on a nickel substrate, it is suggested that the self-discharge of the $NiOOH/Ni(OH)_2$ electrode is mainly due to electrochemical oxidation of hydrogen on the active electrode material.

The self-discharge of the $Ni\text{-}H_2$ battery has been investigated by several researchers with various methods, such as measuring the pressure drop in a battery on open circuit (1, 2), open-circuit potentials (3), and measuring the heat generation rate of the $NiOOH/Ni(OH)_2$ electrode in hydrogen environment (4), and by using the ac impedance technique (5). Three possible mechanisms of the self-discharge process have been proposed in these studies. The first mechanism involves electrochemical oxidation of dissolved hydrogen on the $NiOOH/Ni(OH)_2$ surface or on the sinter nickel substrate with simultaneous electrochemical reduction of nickel oxyhydroxide (NiOOH) to nickel hydroxide [$Ni(OH)_2$] (6). This mechanism allows localized hydrogen oxidation and uniform reduction of nickel oxyhydroxide in the direction perpendicular to the electrode geometric surface. The second mechanism is the direct chemical reaction between dissolved hydrogen and nickel oxyhydroxide (4), in which the local hydrogen oxidation rate must be equal to the reduction rate of nickel oxyhydroxide to nickel hydroxide. The last mechanism (7) includes the oxidation of water into oxygen by nickel oxyhydroxide reduction and recombination of the resulting oxygen with hydrogen to form water on the platinum catalyst in the anode of a $Ni\text{-}H_2$ battery.

The pressure drop in a $Ni\text{-}H_2$ battery on open circuit is a good and accurate indication of the capacity loss due to self-discharge, but it only provides information about the self-discharge in an integral form. Although such data can be analyzed to determine the reaction mechanism by using mathematical models and a model discrimination process, such a procedure does not provide direct evidence for a certain type of reaction mechanism. If the pressure drop data were to be analyzed in conjunction with the nickel electrode potential and the state of charge, it should be possible to determine which mechanism is controlling. Unfortunately, to the best of our knowledge, such an analysis has not been reported. The microcalorimetric technique has many advantages over other techniques because it measures accurately *in situ* the self-discharge rate. However, the investigations using this technique reported so far have been limited to measuring the heat generation rates of single $NiOOH/Ni(OH)_2$ electrodes in a hydrogen environment without simultaneously monitoring the electrode potential and the state of charge. The analysis of such microcalorimetric data can reach only limited conclusions. For example, the heat generation rate of a small nickel electrode is simply too small to be measured accurately if the self-discharge is due to the reaction

$$2NiOOH + H_2O \rightarrow 2Ni(OH)_2 + \frac{1}{2}O_2 \qquad [1]$$

because the enthalpy change for this reaction is about -1.933 kJ/mol,[1] compared to -144.45 kJ/mol for the reaction

$$NiOOH + \frac{1}{2}H_2 \rightarrow Ni(OH)_2 \qquad [2]$$

Measuring the open-circuit potential provides only qualitative information about the self-discharge rates under different conditions. This technique cannot be used to determine the hydrogen oxidation rate nor the nickel reduction rate. Transient techniques such as ac impedance can be used to measure only the current due to $NiOOH/Ni(OH)_2$ redox reaction because this reaction is quite reversible; consequently, these techniques can be used to determine the effect of hydrogen presence on the stability of the

* Electrochemical Society Active Member.

[1] The enthalpy change was estimated using the standard electrode potential data and the method presented in Ref. (6).

nickel electrode, but they are not suitable for determining the kinetics of hydrogen oxidation on the nickel electrode.

Recently, Mao and White (6) developed a mathematical model of the self-discharge of a Ni-H_2 battery, in which the first self-discharge mechanism described above with hydrogen oxidation on the NiOOH/$Ni(OH)_2$ surface was assumed; it was also assumed that the solid phase is a homogeneous mixture of the NiOOH/$Ni(OH)_2$, whose composition depends on the state of charge. The model predictions of the characteristics of the self-discharge, such as the pressure and self-discharge rate as a function of time and the state of charge, are in agreement with experimental observations. However, experimental data are needed before it can be concluded that their proposed mechanism is correct.

The above analysis of the techniques used in previous investigations indicates that a more direct and reliable method is needed to determine the mechanism of the self-discharge of a NiOOH/$Ni(OH)_2$ electrode in a hydrogen environment. Details about the self-discharge process, particularly concerning the contribution of oxygen evolution, electrochemical or chemical nature of the self-discharge process, and correlations of the self-discharge rate with hydrogen pressure, the state of charge, and the electrode potential need to be investigated further.

In the present work, steady-state currents were measured as a function of the gas pressure in a cell, the electrode potential, or the state of charge for the NiOOH/$Ni(OH)_2$ electrode in hydrogen and argon environments. The self-discharge rates were then correlated with these variables. In addition, to determine the effect of nickel sinter substrate on the self-discharge of the NiOOH/$Ni(OH)_2$ electrode, steady-state currents were measured for bare nickel sinter electrodes as a function of the electrode potential and hydrogen pressure.

Although it is difficult to determine the equilibrium potential of a NiOOH/$Ni(OH)_2$ electrode in alkaline electrolyte because the rest potential is actually a mixed potential of those for oxygen evolution and nickel oxyhydroxide reduction (8, 9), several investigators have reported that the rest potential is a function of the state of charge and follows closely the Nernst equation (10, 11). Therefore, if the electrode potential is kept at a constant value by using a potentiostat, the ratio of NiOOH/$Ni(OH)_2$ in the electrode would be forced to remain a constant value. Consequently, it would be expected that the net current measured at steady state would be zero if there were no species which could be continuously either reduced or oxidized at the given potential. If hydrogen gas is present and it can be electrochemically or chemically oxidized at these potentials, the current measured at steady state would be due to the hydrogen oxidation. If the potential is controlled in a region where oxygen evolution can also occur, the current would include that portion due to oxygen evolution. These two currents can be determined separately by conducting experiments in an inert gas and in a hydrogen environment. The measured steady-state currents would represent the self-discharge rate of the nickel electrode at each potential due to hydrogen oxidation and oxygen evolution. Therefore, by measuring and analyzing the steady-state currents, the self-discharge mechanism of the NiOOH/$Ni(OH)_2$ electrode can be determined as described below.

Experimental

Figure 1 shows a schematic view of the pressure vessel cell used in the experiments. The pressure vessel was made of stainless steel. The chamber was 8 cm in diam and 18 cm in height. The inlet stainless steel tube at the bottom was connected directly to a hydrogen or argon gas cylinder whereas the outlet tube mounted on the cap was blocked during experiments by a dead end Swagelock. It was used to release gas when the electrode or gas needed to be changed. A precise pressure gauge was mounted on the cap to monitor the pressure in the vessel. Three stainless steel bars were mounted on the cap as the leads for the three electrodes (working, counter-, and reference electrodes). They were insulated from one another by ceramic tubes surrounding the bars.

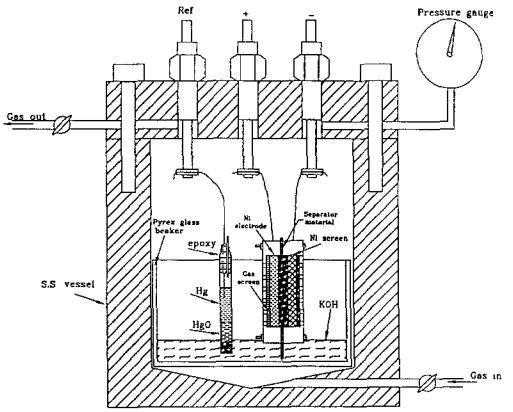

Fig. 1. Schematic view of the pressure vessel and the arrangement of the experimental cell.

The cell that houses the working electrode, separator, and counterelectrode consisted of two pieces of Plexiglas, on which a grove of two square centimeters wide and 0.1 cm deep was machined, and many small uniformly distributed holes were drilled through the back side of the grove to provide a gas path. The two plates were tightly held by four bolts; one at each corner, as shown in Fig. 1. The electrodes were cut to fit into the groves, four layers of porous polyethylene sheet were folded and placed between the nickel electrode and a nickel screen and served as the separator, and the nickel screen served as the counterelectrode. The cell was hung above the electrolyte while part of the separator was in contact with the electrolyte so as to keep the electrodes wet via capillary action. The reference electrode was a Hg/HgO electrode in the same electrolyte. A small segment of Pyrex glass tube (1/16 in. od) was used to make the reference electrode. One end of the glass tube was blocked with the pressed polyethylene to prevent HgO paste from falling off the tube and to allow contact between the electrolyte and HgO. The HgO paste was prepared using the same electrolyte and HgO powder. After the HgO paste was added to the bottom part of the tube, mercury was poured on top of it. The other end of the tube was sealed by epoxy to keep the platinum wire lead and small plastic tube in place as shown in Fig. 1. This plastic tube provides a means of regulating the pressure to balance the pressure between the inside and outside of the tube. This yields a stable electrode potential when the vessel pressure is changed.

The electrodes used in the experiments were provided by Hughes Aircraft Company. They were prepared by impregnating nickel hydroxide into nickel sinter plaque using an electrochemical method. The electrode contained about 6 weight percent (w/o) Co, was 0.075 cm thick, and had a capacity of about 25 mAh/cm^2. The electrolyte used in all of the experiments was 31 w/o KOH solution. A potentiostat/galvanostat, PAR Model 273, was used to control the electrode potential difference between the working electrode and the reference electrode. Currents were recorded on a X-t recorder, Hewlett-Packard Model 7132A. Zero grade hydrogen and argon gas were used in the experiments and the electrolyte was prepared using deionized water and analytically pure potassium hydroxide pellets.

After the cell had been placed in the pressure vessel, argon gas was flushed through the vessel to purge the air. The electrode was then fully charged and discharged at a rate of about C/10 (10 mA total current) until the electrode capacity became stable (usually after four cycles). The electrode was finally charged to the full capacity and rested on open circuit for a certain period of time (long enough so that the electrode potential did not change more than 1 mV for 1 h). The electrode potential was then controlled at the rest potential, and the corresponding current was recorded until it reached steady state (*i.e.*, the current did not change during the course of 1 h). The time required for the currents to reach steady state varied from 3 h to more than 15 h, depending on the state of charge and on

whether only the gas pressure was changed or both the electrode potential and the gas pressure were changed. It usually took longer in the middle region of the state of charge than at both the ends of the state of charge to reach steady state. It was also observed that in the middle region of the state of charge the current oscillated slightly; the recorded current formed a band with a certain width. When this happened, the average value was taken for the steady-state current. It is believed that this oscillation phenomenon is due to the intrinsic character of this particular system under the potentiostatic control where a highly reversible reaction ($NiOOH/Ni(OH)_2$) is nearly at an equilibrium state whereas the other reaction (hydrogen oxidation) is kinetically slow and far from its equilibrium state (12). Under these conditions, a random disturbance to the electrode potential would result in an appreciable reaction rate for the nickel redox reaction, thereby causing an oscillating current.

When one gas was changed to another one (from argon to hydrogen, or vice versa), the vessel was flushed with the second gas for about 10 min before the outlet was closed and the gas pressure was raised to the desired value. After the current measurements for each constant potential for different pressures of both argon and hydrogen gas were completed, a desired amount of capacity was discharged at C/10 rate (10 mA) and the cell was returned to open circuit again for the electrode potential to reach a new steady value. The electrode potential was then controlled at this new value while the current was recorded. These steps were repeated until the electrode was completely discharged.

Results and Discussion

Figure 2 presents the steady-state currents measured *vs.* argon pressure for the $NiOOH/Ni(OH)_2$ electrode at different electrode potentials. It was observed that the electrode potential on open circuit was not stable above 0.4 V; it would fall gradually to a value below 0.4 V. To measure the currents at potentials higher than 0.4 V, the electrode was charged galvanostatically at 10 mA to the vicinity of a desired potential, and then the operational mode of the potentiostat was changed immediately to potentiostatic. The corresponding current was measured at steady state. Figure 2 shows that the currents are nearly independent of pressure and become almost zero at the potential of 0.303 V. Since the currents measured are anodic current, in an argon environment, the possible reaction for the measured anodic current is the oxidation of hydroxide ions into oxygen gas

$$4\,OH^- - 4e^- \rightarrow O_2 \uparrow + 2H_2O \qquad [3]$$

The reversible electrode potential for this reaction is approximately 0.30 V *vs.* Hg/HgO in the same electrolyte for an O_2 pressure of 1 atm; the actual value under the experimental condition may be lower because the oxygen partial pressure is lower. However, Fig. 2 shows that the reaction rate becomes appreciable only when the electrode potential is higher than 0.4 V. Therefore, it can be inferred that a $NiOOH/Ni(OH)_2$ electrode would rapidly lose its capacity due to oxygen evolution when the electrode is fully charged and the electrode potential is higher than 0.4 V. It was observed that more than 95% of the initial capacity still remained when the electrode potential fell below 0.4 V. Therefore, it is unlikely that oxygen evolution is the main cause for the self-discharge of a $NiOOH/Ni(OH)_2$ electrode in a hydrogen environment because the electrode potential is below 0.4 V *vs.* Hg/HgO; in addition, the measured currents in this experiment were small compared to actual self-discharge current in a hydrogen environment. If the capacity loss is about 10% of its total capacity per day for a fully charged electrode in an actual battery, the self-discharge current would be about 0.417 mA for the electrode used in this experiment, which is much higher than the measured anodic current (0.071 mA) at 0.4 V. Consequently, other reactions must contribute to the self-discharge of the Ni/H_2 battery.

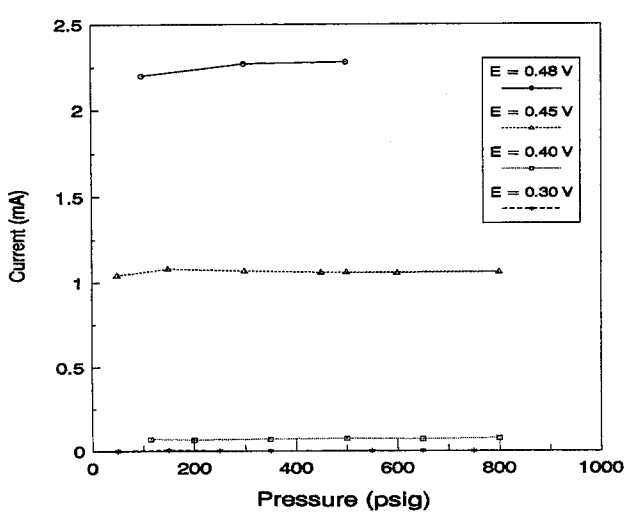

Fig. 2. The steady-state anodic current *vs.* argon pressure for the $NiOOH/Ni(OH)_2$ electrode at four electrode potentials. The total geometric electrode area was 4 cm^2.

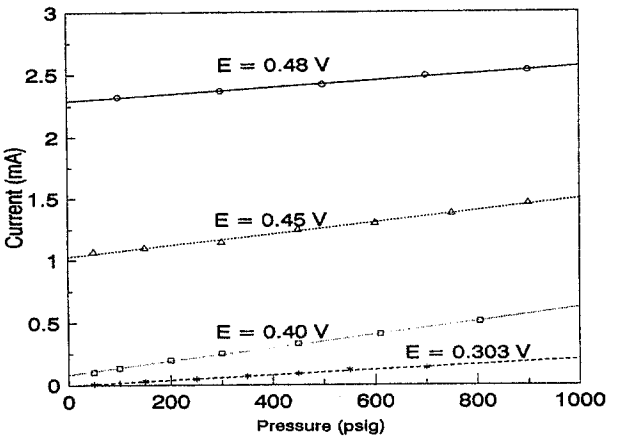

Fig. 3. The steady-state anodic current as a function of hydrogen pressure for the $NiOOH/Ni(OH)_2$ electrode at four electrode potentials.

In contrast to Fig. 2, the anodic currents on the $NiOOH/Ni(OH)_2$ electrode increase proportionally with hydrogen pressure at any electrode potential as shown in Fig. 3. Since the curves do not pass through the origin of the axes and they are nearly parallel, the total current must result from the oxidation of both hydrogen and hydroxide ions, the latter being independent of the hydrogen pressure. Therefore, by subtracting the current measured in an argon environment, the portion of the current due to hydrogen oxidation can be obtained. Figure 4 shows the hydrogen oxidation current as a function of hydrogen pressure at different potentials; the plots are linear and almost pass through the origin of the axes. It can be inferred that the self-discharge due to hydrogen oxidation can be reduced to a minimum value by substantially decreasing the hydrogen pressure.

If the anodic currents are due to the direct chemical reaction between dissolved hydrogen and nickel oxyhydroxide while the resulting nickel hydroxide was simultaneously electrochemically converted back to nickel oxyhydroxide, it would be expected that the anodic currents would vary proportionally with the state of charge, and would be less dependent on the electrode potential. If the anodic currents are due to the electrochemical oxidation of dissolved hydrogen, the logarithm of the anodic currents would vary linearly with the electrode potential. Figure 5 presents the anodic currents measured on a logarithm scale and the electrode potential for different hydrogen pressures. It is quite clear that these curves are nearly linear, and consequently, they indicate that the hydrogen is electrochemically oxidized. Figure 5 also shows that the slopes of the curves are almost the same, indicating that the reaction mechanism is the same at all pressures.

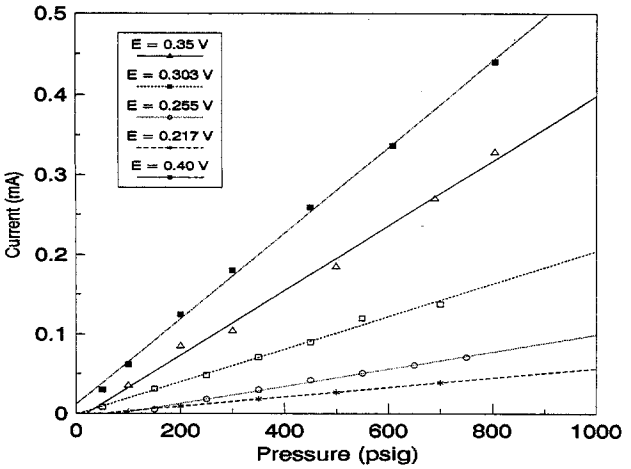

Fig. 4. The hydrogen oxidation current *vs.* hydrogen pressure for the $NiOOH/Ni(OH)_2$ electrode. The y axis represents the current differences between those separately measured in hydrogen and argon environments.

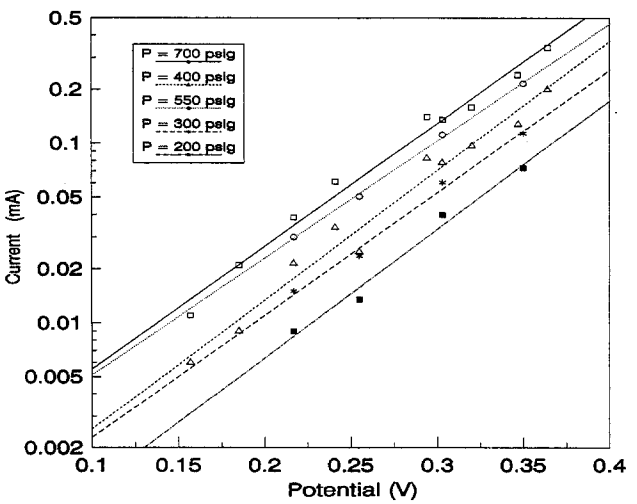

Fig. 5. The hydrogen oxidation current as a function of the electrode potential for the $NiOOH/Ni(OH)_2$ electrode at different hydrogen pressures.

To clarify whether the anodic current has a distinct relationship with the state of charge, the measured anodic currents were plotted as a function of the discharged capacity. Figure 6 presents these plots. Although the current decreases with the discharged capacity, it is difficult to interpret the relationship between the current and the discharge capacity based on the chemical reaction mechanism because the slopes of the curves vary from one region to another. A plot of the electrode potential *vs.* the discharged capacity for the same data presented in Fig. 6 is given in Fig. 7. It can be seen by comparing Fig. 6 and 7 that the anodic current and the potential have a similar trend as a function of the discharged capacity. Therefore, it may be concluded that the hydrogen oxidation rate depends strongly on the electrode potential but not on the capacity.

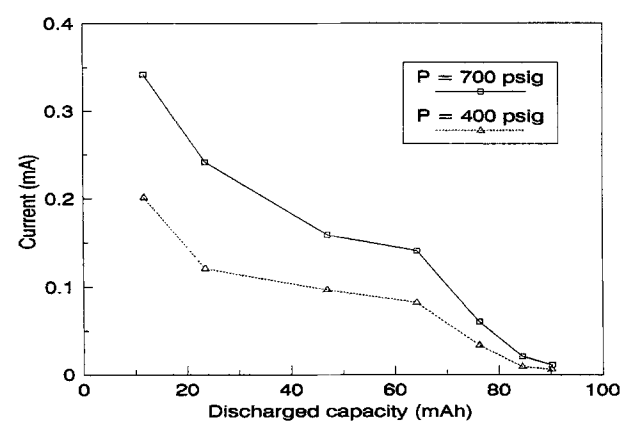

Fig. 6. The hydrogen oxidation current as a function of the discharged capacity for the $NiOOH/Ni(OH)_2$ electrode. The total capacity of the electrode was about 100 mAh determined from a discharging curve at 10 mA.

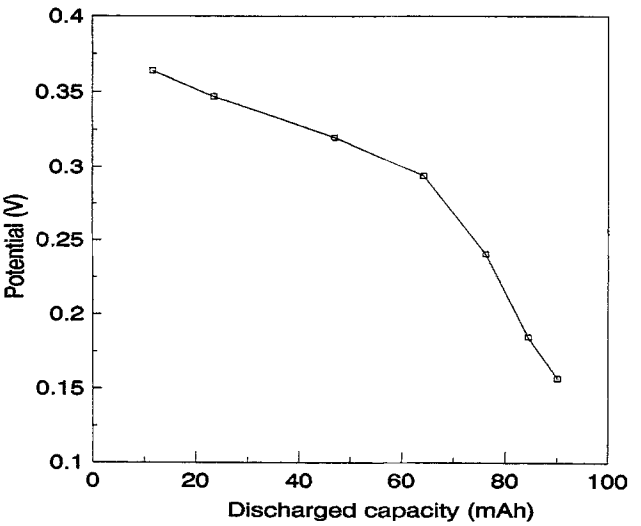

Fig. 7. The rest potentials *vs.* the discharged capacity. The open square symbols show the potentials where those hydrogen oxidation currents in Fig. 6 were measured.

The linear plots shown in Fig. 5 indicate that the relationship between the hydrogen oxidation current and the electrode potential can be expressed by the Tafel equation

$$i = a \exp(bE) \quad [4]$$

where E represents the electrode potential in volts, the reciprocal of the symbol b is normally referred to as the Tafel slope, and a may be considered as the reaction rate constant. In order to extract an apparent exchange current density from Fig. 5, one must know the equilibrium potential for each pressure and rearrange Eq. [4] to

$$i = Ax_s a_s K P^{\alpha} \exp(bE_{eq}) \exp[b(E - E_{eq})] \quad [5]$$

where the symbols A, x_s, and a_s represent the projected surface area, the thickness of the electrode, and the electroactive surface area per unit volume of the electrode, respectively. The symbol K represents a constant. The exchange current density is defined here as

$$j_o = KP^{\alpha} \exp(bE_{eq}) \quad [6]$$

and b is normally expressed as a function of temperature

$$b = \frac{\beta F}{RT} \quad [7]$$

where β is referred to as a transfer coefficient. The reaction rate constant a in Eq. [4] and the calculated exchange current densities for each pressure are given in Table I. The average slope of the curves in Fig. 5 and the equilibrium potentials presented in Fig. 10 were used in calculating these exchange current densities. Nonlinear regression of the above equation (Eq. [5]) with the data for K and α yields $\alpha = 1.00$. Since the equilibrium potential is also a function of hydrogen pressure, j_o can be expressed as

$$j_o = k_o P^{\gamma} \quad [8]$$

By using the values for j_o in Table I and P, it was obtained that $k_o = 8.93 \times 10^{-18}$ and $\gamma = 0.8$ for pressure in psia and j_o in A/cm^2. These data confirm further that the hydrogen oxidation is a slow process, and the reaction order with respect to hydrogen pressure is unity.

Table I. Apparent exchange current densities.

Pressure (psig)	b (V^{-1})	a (mA)	j_o (A/cm^2)[a]
700	15.7684	1.1398×10^{-3}	1.48×10^{-15}
550	15.0395	1.1329×10^{-3}	1.54×10^{-15}
400	15.1618	7.615×10^{-4}	1.10×10^{-15}
300	14.2352	6.995×10^{-4}	1.07×10^{-15}
200	15.0318	3.368×10^{-4}	5.58×10^{-16}

[a] The following values were used in calculating these parameters: $a_s = 10^3$ cm^2/cm^3, $x_s = 0.075$ cm, and $A = 4.0$ cm^2. The equilibrium electrode potential potential for each pressure was calculated based on the equation obtained from Fig. 10

$$E_{eq} = -0.8926 - 0.0134 \ln (P) \text{ V}$$

where the pressure P is psia.

The above analysis of the kinetic data was based on the assumption that the oxidation of dissolved hydrogen is kinetically controlled without any mass transport effect. Since the electrodes used were porous and had a high specific surface area, the true exchange current density for hydrogen oxidation on a flat $NiOOH/Ni(OH)_2$ may be much different from those calculated above. In order to estimate the kinetic parameters correctly, it is important to know the degree of mass-transfer effect on the polarization curves. If the thickness of the electrolyte film covering the electrode and the true specific surface area of the electrodes are known, a macrohomogeneous approach can be used to obtain the polarization equation and further to estimate the exchange current density for a flat electrode. A simple model for the hydrogen oxidation process under such an experimental condition is presented in the Appendix. With the parameters listed in Table A-1 the exchange current density and transfer coefficient (β) were estimated to be 3.00×10^{-16} A/cm^2 and 0.425, compared to 1.48×10^{-15} A/cm^2 and 0.405 calculated without considering the effect of mass transfer. The exchange current density for a flat electrode is about one order of magnitude smaller than those listed in Table I, but the transfer coefficient is close to the theoretical value of 0.5 for the mechanism of electron transfer as the controlling step for hydrogen oxidation (13). These differences may be due to the effect of mass transport.

The experimental data presented so far indicate that hydrogen oxidation is an electrochemical reaction, but it is still unclear whether hydrogen oxidation occurs on the exposed nickel substrate or on the active material. Since a nickel substrate is subjected to positive polarization when the electrode is under charged state and pure nickel is not stable in alkaline solution, the surface property of a nickel substrate may be much different from that of pure nickel. Therefore, it is essential to measure the hydrogen oxidation current on a bare nickel sinter at different potentials to determine the effect of the nickel substrate on the self-discharge. In this set of experiments, the nickel sinter plaque used was also provided by Hughes Aircraft Company. The experiments were started with a fresh bare sinter nickel electrode at its open-circuit potential, and the electrode potential was changed step by step in the positive direction. Figure 8 shows the results of these measurements. It can be seen that the hydrogen oxidation current increases rapidly with the electrode potential from the open-circuit potential, reaches a maximum value, and then decreases sharply. A possible explanation is that the surface of the electrode is oxidized to nickel hydroxide and a passivation film is formed when the potential becomes more positive than −0.7 V relative to the Hg/HgO electrode. Such a passivation film strongly inhibits hydrogen oxidation. If this explanation is true, it follows that the nickel substrate in a $NiOOH/Ni(OH)_2$ electrode would not have a significant role in the self-discharge process. In other words, the hydrogen oxidation on the $NiOOH/Ni(OH)_2$ electrode occurs predominantly on the active material. When the passivation film has been formed, it is difficult to remove it electrochemically or convert it back to the original nickel. Figure 9 shows the hydrogen oxidation current as a function of time at a potential of

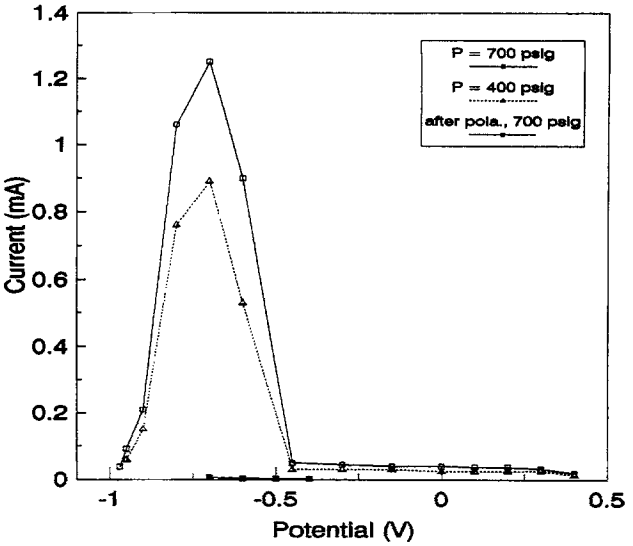

Fig. 8. The steady-state anodic current vs. the electrode potential for a bare nickel sinter electrode in hydrogen environments. The solid square symbol represents the current for the same electrode after it had undergone a positive polarization up to 0.4 V. No steady state could be obtained at a potential more negative than 0.75 V if the electrode has been polarized at a positive potential.

−0.8 V for a bare nickel sinter which was previously polarized. The current continuously increases with time, but very slowly. This slow increase in the current is explained as a slow conversion process of nickel hydroxide into original nickel which enables the surface to gain gradually catalytic activity for hydrogen oxidation. In contrast to this slow increase in the current, the current would decrease and reach steady state within about 3 h for a fresh electrode.

Although the surface property has changed after the nickel sinter is polarized, the open-circuit potential is not affected as shown in Fig. 10. The open-circuit potentials were almost the same before and after the electrode was oxidized. The excellent linear relationship between the logarithm of the open-circuit potential and the hydrogen pressure and the fitting value of the slope (0.0134 V at room temperature) indicate that the open-circuit potential agrees well with the theoretical equation for the equilibrium potential of hydrogen redox

$$E_{eq} = E^{\circ}_{eq} - \frac{RT}{nF} \ln P \qquad [10]$$

where n is equal to 2 and hydrogen gas behaves like an ideal gas.

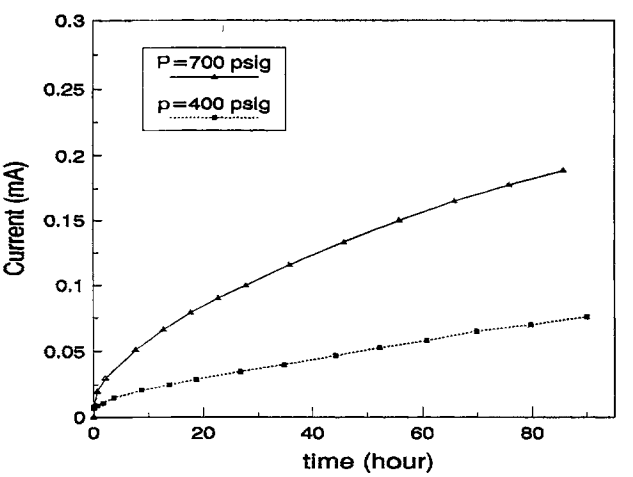

Fig. 9. The anodic current as a function of time at $E = -0.8$ V for the bare nickel sinter electrode at two hydrogen pressures. The electrode was previously polarized at 0.35 V for 2 h.

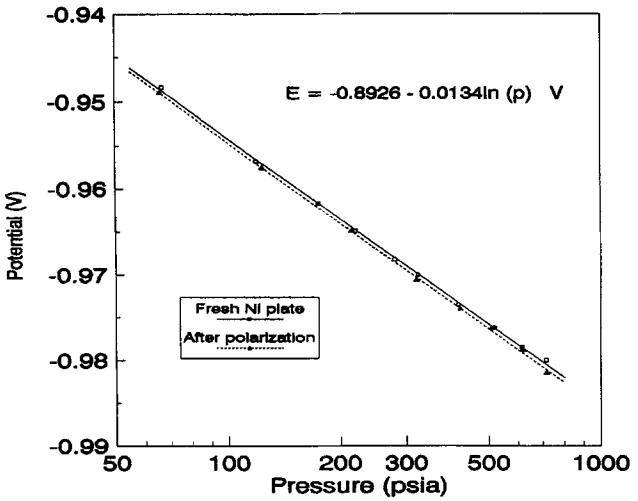

Fig. 10. The steady-state potential vs. pressure for the bare nickel sinter electrode on open circuit in hydrogen environments. The open square symbol represents the potentials of a fresh electrode, the solid triangle symbols represent potentials obtained after the electrode subjected to a positive polarization.

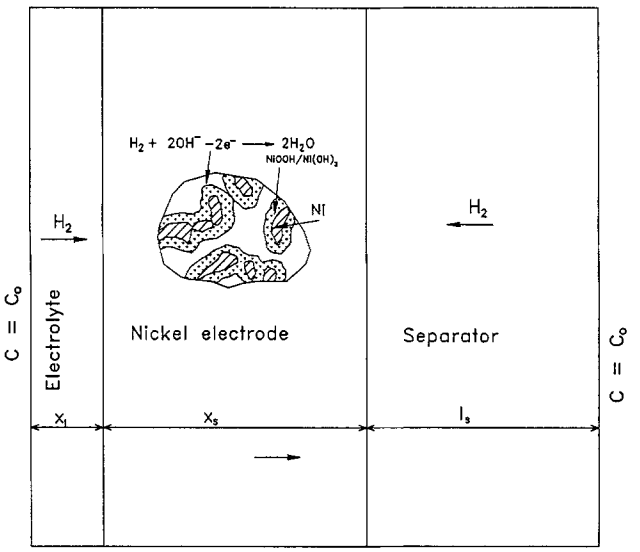

Fig. A-1. A schematic view of the hydrogen oxidation process on the nickel electrode.

Conclusions

A constant potential method has been shown to be an effective tool to determine directly the self-discharge rate of the $NiOOH/Ni(OH)_2$ electrode under various conditions. The self-discharge of the $NiOOH/Ni(OH)_2$ electrode in a hydrogen environment is mainly due to electrochemical oxidation of dissolved hydrogen with simultaneous reduction of nickel oxyhydroxide. Oxygen evolution which is considerable only at high potentials, contributes little to the self-discharge. The hydrogen oxidation occurs predominantly on the active material and is a first-order reaction with respect to hydrogen pressure. The oxidized form of the nickel substrate shows a great inhibition to the electrochemical oxidation of dissolved hydrogen.

Acknowledgments

This work was financed by the Hughes Aircraft Company and the NASA Center for Space Power at Texas A&M University. Valuable discussions with Dr. Hong Lim of the Hughes Aircraft Company are gratefully acknowledged. Some assistance in the experiments from Mr. Junbom Kim of our research group is appreciated.

Manuscript submitted June 28, 1991; revised manuscript received Nov. 27, 1991.

Texas A&M University assisted in meeting the publication costs of this article.

APPENDIX

Estimation of the Exchange Current Density

Dissolved hydrogen is oxidized at the $NiOOH/Ni(OH)_2$ electrode according to the reaction

$$H_2 + 2\,OH^- - 2e \rightarrow 2H_2O \qquad [A\text{-}1]$$

The reaction at the counterelectrode (nickel screen) must be hydrogen evolution, the reverse of [A-1]. It is reasonable to assume that the concentration of dissolved hydrogen at the interface between the electrolyte/hydrogen gas phase and at the counterelectrode is at equilibrium with its gas pressure. Figure A-1 shows a schematic of the hydrogen oxidation process under this experimental condition.

Since the current passing through the cell is relatively small and no external force would cause the electrolyte to flow, the dissolved hydrogen transfer from the gas-electrolyte interface to the $NiOOH/Ni(OH)_2$ electrode may be only due to diffusion. Therefore, Fick's equation is used. In the electrolyte film ($0 < x < x_1$) and in the separator ($x_1 + x_s < x < x_1 + x_s + l_s$), the dissolved hydrogen is neither produced nor consumed. The diffusion equations for these regions at steady state are as follows

$$D\frac{d^2C}{dx^2} = 0 \qquad 0 < x < x_1 \qquad [A\text{-}2]$$

$$D_2\frac{d^2C}{dx^2} = 0 \qquad x_1 + x_s < x < x_1 + x_s + l_s \qquad [A\text{-}3]$$

where the symbols, D and D_2, represent the effective diffusion coefficients of dissolved hydrogen in the electrolyte film and in the separator, respectively. The dissolved hydrogen is oxidized while it diffuses within the electrode. Consequently, the diffusion equation becomes

$$D_1\frac{d^2C}{dx^2} - \frac{a_s j}{2F} = 0 \qquad [A\text{-}4]$$

where D_1 is the effective diffusion coefficient in the electrode and a_s is the electroactive surface area per unit volume of the nickel electrode. Both D_1 and a_s may change with the state of charge or the electrode potential. However, they are assumed here to be constant for simplicity. The symbol j represents the current density due to hydrogen oxidation, which may be expressed by the equation

$$j = j_{o,ref}\left(\frac{C}{C_{ref}}\right)\exp\left[\frac{\beta F}{RT}(E - E_{ref})\right] \qquad [A\text{-}5]$$

The analytical solution of the above equations can be easily obtained for the constant boundary condition,

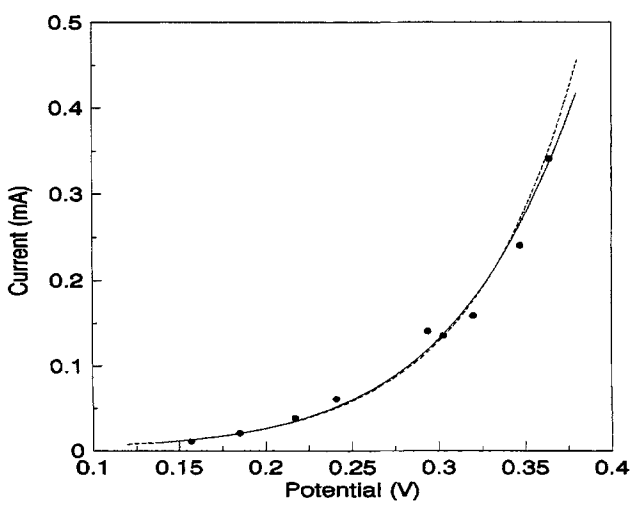

Fig. A-2. The hydrogen oxidation current as a function of the electrode potential for the $NiOOH/Ni(OH)_2$ electrode in a hydrogen environment, P = 700 psig. The dashed line represents the best fit by Eq. [4], and the solid line represents the best fit by Eq. [A-7], using the parameters in Table A-1.

Table A-I. Input parameters.

A	4.0 cm
a_s	1.0×10^3 cm^2/cm^3
C_o	$=6.86 \times 10^{-7} P$ exp [(−0.315 × 8.0)] mol/cm^3, P in atm (14)
C_{ref}	$= C_o$
D	1.5×10^{-5} cm^2/s
D_1	$=D\epsilon_e^{1.5}$
D_2	$=D\epsilon_s^{1.5}$
F	96,487 C/mol
$i_{o,ref}$	2.90×10^{-16} A/cm^2
P	714.696 psia
R	8.314 J/mol-K
T	295.15 K
x_1	10 μm
x_s	0.075 cm
l_s	0.01 cm
β	0.425
ϵ_e	0.65
ϵ_s	0.75

$C = C_o$, at both $x = 0$ and $x = x_1 + x_s + l_s$. The concentration distribution in the NiOOH/Ni(OH)$_2$ electrode is given as follows

$$C = C_o \left\{ \frac{f_1}{f} \exp(-\sqrt{B}x) + \frac{f_2}{f} \exp(-\sqrt{B}x) \right\} \quad [A\text{-}6]$$

where x varies from 0 to x_s and

$$B = \frac{a_s j_{o,ref}}{2FD_1C_{ref}} \exp\left[\frac{\beta F}{RT}(E - E_{ref})\right]$$

$$f_1 = \frac{D}{x_1D_1\sqrt{B}}\left(1 - \frac{D_2}{l_sD_1\sqrt{B}}\right) \exp(-\sqrt{B}x_s) + \frac{D_2}{l_sD_1\sqrt{B}}\left(1 + \frac{D}{x_1D_1\sqrt{B}}\right)$$

$$f_2 = \frac{D}{x_1D_1\sqrt{B}}\left(1 + \frac{D_2}{l_sD_1\sqrt{B}}\right) \exp(-\sqrt{B}x_s) - \frac{D_2}{l_sD_1\sqrt{B}}\left(\frac{D}{x_1D_1\sqrt{B}} - 1\right)$$

$$f = \left(\frac{D}{x_1D_1\sqrt{B}} - 1\right)\left(1 - \frac{D_2}{l_sD_1\sqrt{B}}\right) \exp[-\sqrt{B}x_s] + \left(\frac{D}{x_1D_1\sqrt{B}} + 1\right)\left(1 + \frac{D_2}{l_sD_1\sqrt{B}}\right) \exp[\sqrt{B}x_s]$$

where l_s and x_1 represent the thickness of the separator and the electrolyte film, as shown in Fig. A-1.

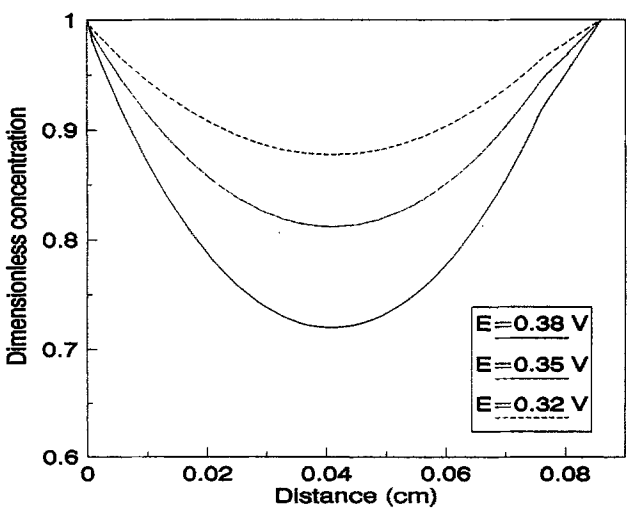

Fig. A-3. Predicted concentration distributions for dissolved hydrogen. The parameters used are listed in Table A-1.

The total current for a given potential equals the integration of the transfer current density multiplied by the geometric projected surface area

$$i = Aa_s \int_o^{x_s} j dx = \frac{Aa_s i_{o,ref} C_o}{C_{ref}\sqrt{B}} \exp\left[\frac{\beta F}{RT}(E - E_{ref})\right] \left\{ \frac{f_1}{f}[\exp(-\sqrt{B}x_s) - 1] - \frac{f_2}{f}[\exp(-\sqrt{B}x_s) - 1] \right\} \quad [A\text{-}7]$$

where A represents the total projected surface area (4 cm^2).

Since the polarization equation derived is quite complicated, it is difficult to discuss the potential-current relationship without plotting the equation. Figure A-2 represents such a plot in which the parameters listed in Table A-1 were used and $i_{o,ref}$ and β are the values giving Eq. [A-7] the best fit to the experimental data. Although the fitting curves by Eq. [A-7] and [4] almost overlap in the low potential region, the two curves deviate from each other in the high potential region, possibly because of the mass transport effect. Figure A-3 shows the predicted concentration distribution for dissolved hydrogen at different potentials. It can be seen that depletion of the dissolved hydrogen concentration in the electrode is appreciable when the electrode potential is increased.

LIST OF SYMBOLS

A	projected nickel electrode surface area, cm^2
a	pre-exponential constant in Eq. [4], mA
a_s	electroactive surface area per unit volume of the nickel electrode, cm^2/cm^3
b	Tafel slope given in Eq. [4], V^{-1}
C	concentration of dissolved hydrogen, mol/cm^3
C_o	the concentration of dissolved hydrogen at the interface between hydrogen gas and the electrolyte, mol/cm^3
C_{ref}	reference concentration of dissolved hydrogen, mol/cm^3
D	effective diffusion coefficient of dissolved hydrogen, cm^2/s
D_1	effective diffusion coefficient of dissolved hydrogen in the nickel electrode, cm^2/s
D_2	effective diffusion coefficient of dissolved hydrogen in the separator, cm^2/s
E	the nickel electrode potential in solid phase, V
E_{ref}	the equilibrium electrode potential for hydrogen oxidation at a reference state, V
$E_{eq.}$	the equilibrium electrode potential for hydrogen oxidation at a given hydrogen pressure, V
$E^o_{eq.}$	the equilibrium electrode potential for hydrogen oxidation at a hydrogen pressure of 1 atm, V
F	Faraday constant, 96,487 C/mol
i	total current, mA
j_o	exchange current density for hydrogen oxidation evaluated at a given hydrogen pressure, A/cm^2
$j_{o,ref}$	exchange current density for hydrogen oxidation evaluated at a reference state, A/cm^2
j	local current density due to hydrogen oxidation, A/cm^2
l_s	separator thickness, cm
K	reaction rate constant for hydrogen oxidation in Eq. [6], A/cm^2-psia$^{-\alpha}$
k_o	reaction rate constant for hydrogen oxidation given in Eq. [8], A/cm^2-psia$^{-\gamma}$
P	hydrogen pressure, psia
R	universal gas constant, 8.314
T	temperature, K
x	spatial coordinate, cm
x_s	the nickel electrode thickness, cm
x_1	the thickness of an electrolyte film covering the nickel electrode, cm
α	reaction order with respect to hydrogen pressure given in Eq. [5]
β	anodic transfer coefficient for hydrogen oxidation
γ	reaction order with respect to hydrogen pressure given in Eq. [8]
ϵ_e	the porosity of the nickel electrode
ϵ_s	the porosity of the separator

REFERENCES

1. G. Holleck, in "Proceedings of 1977 Goddard Space Flight Center Battery Workshop," p. 525, NASA Conf. Pub. 2041 (1977).
2. P. E. Ritterman and A. M. King, in "Proceedings of the

20th Intersociety Energy Conversion Engineering Conference, p. 1.175 (Aug. 1985).
3. Y. J. Kim, S. Srinivasan, and A. J. Appleby, *J. Appl. Electrochem.*, **20,** 377 (1990).
4. Y. Kim, A. Visintin, S. Srinivasan, and A. J. Appleby, in "Proceedings of the Symposium on Nickel Hydroxide Electrodes," D. A. Corrigan and A. H. Zimmerman, Editors, PV 90-4, p. 368, The Electrochemical Society Softbound Proceedings Series, Pennington, NJ (1990).
5. K. A. Murugesamoorthi, Y. J. Kim, S. Srinivasan, and A. J. Appleby, Abstract 82, p. 124, The Electrochemical Society Extended Abstracts, Vol. 88-2, Chicago, IL, Oct. 9-14, 1988.
6. Z. Mao and R. E. White, *This Journal,* **138,** 3354 (1991).
7. C. Iwakura, Y. Kajiya, H. Yoneyama, T. Sakai, K. Oguro, and H. Ishikawa, *ibid.,* **136,** 1351 (1989).
8. R. Barnard, C. F. Randell, and F. L. Tye, *J. Appl. Electrochem.*, **10,** 127 (1980).
9. J. McBreen, in "Modern Aspects of Electrochemistry," R. E. White, J. O'M. Bockris, and B. E. Conway, Editors, p. 29, Plenum Press, New York (1990).
10. K. Micka and I. Rousar, *Electrochim. Acta,* **25,** 1085 (1980).
11. J. Bouet, F. Richard, and Ph. Blanchard, in "Proceedings of the Symposium on Nickel Hydroxide Electrodes," D. A. Corrigan and A. H. Zimmerman, Editors, PV 90-4, p. 260, The Electrochemical Society Softbound Proceedings Series, Pennington, NJ (1990).
12. J. Wojtowicz, in "Modern Aspects of Electrochemistry," J. O'M. Bockris and B. E. Conway, Editors, p. 47, Plenum Press, New York (1972).
13. J. O'M. Bockris and A. K. N. Reddy, "Modern Electrochemistry," Vol. 2, Plenum Press, New York (1977).
14. S. G. Bratsch, *J. Phys. Chem. Ref. Data,* **18,** 1 (1989).

Electroless Ni-P Deposition on Silicon with Pd Activation

Valery M. Dubin

Minsk Radioengineering Institute, 220600 Minsk, Byelorussia, Union of Soviet Socialist Republics

ABSTRACT

The electroless Ni-P deposition on silicon with Pd activation was investigated by Rutherford backscattering spectrometry (RBS) and electron microscopy. An "RBS double-layer" structure SiPdNiP/NiP with different composition was simulated to evaluate the composition profiles of the films produced by electroless NiP deposition with Pd activation. During deposition on Si with Pd activation, the initially formed NiP alloy was found to contain approximately two times more P than that formed after long deposition times. To explain the distribution of P in NiP alloy suggested that the catalytic properties of the surface change during the deposition process. The thickness of the SiPdNiP layer also changes during NiP deposition. It was observed that the maximum thickness of SiPdNiP layer ranges from 2400 to 2500 Å. Contact hole to silicon device with a 0.5 μm depth p-n junctions and a 1.5 μm nominal sizes were filled by NiP after Pd activation. The contact resistivity on n-type silicon ($R_s = 40 \pm 10\ \Omega/\square$ and $N = 3 \cdot 10^{19}\ cm^{-3}$) was in the $10^{-8}\ \Omega \cdot cm^2$ range after a 450°C nitrogen annealing cycle for 30 min.

Investigations of electroless Ni-P deposition on silicon with Pd activation are very important not only from the academic point of view for a better understanding of mechanisms of electroless Ni-P deposition, but also from a technological point of view because Ni-P films can be applied for ohmic contacts with silicon in semiconductor devices and for contact filling in very large scale integrated (VLSI) chips (1). It is now generally agreed that electroless and electrodeposited Ni-P films are not homogeneous but consist of regions with different phosphorus contents and structures (2-5). The variation in composition has previously been explained in terms of the fluctuations of the pH at the alloy/electrolyte interface during the deposition. However, whatever the reasons are, the fluctuations of the pH at the alloy/electrolyte interface occur during the deposition process and the question remains as to why in some cases narrow layers of different composition appear parallel to the NiP/substrate interface. The answers to these fundamental questions have not been found yet.

Pd is widely used in order to activate dielectric, semiconductor, or metal surfaces before electroless metal deposition. However, the role of the Pd activation process and Pd catalytic properties with respect to the reactions of Ni and P reduction still remains largely unclear. Investigations of the P distribution in the Ni-P alloy obtained after Pd activation has not previously been reported. Last but not least, for technological purposes it is necessary to know how the thicknesses of the layers obtained by electroless NiP deposition on silicon with Pd activation and their composition depend on the specific experimental conditions.

Experimental

High-purity n-type silicon (0.05 Ω · cm) with dimensions of 10 × 10 × 0.4 mm and with class 14 of surface roughness were used as substrates. The silicon surface was activated before Ni-P deposition. The composition of a Pd activation solution is given in Table I. Bath compositions for Ni-P deposition are given in Table II.

Using high-resolution transmission electron microscopy (TEM), structural investigations of NiP films were performed. Amorphous structures were identified from structureless micrographs indicating lack of crystalline grain boundaries and the absence of crystalline diffraction rings. The compositions and total thicknesses of NiP films were determined using Rutherford backscattering spectrometry (RBS). The compositions and the thicknesses at various depths were estimated using a simulation program and comparison with the experimentally obtained RBS-

Table I. Composition of the Pd activation solution.

Chemicals	Concentration ($ml \cdot l^{-1}$)
$PdCl_2$	$1\ g \cdot l^{-1}$
HCl	1
HF (48%)	449

Table II. Bath compositions and conditions for NiP alloy deposition. Parameters for deposition: temperature, 50°C; pH = 6.0 and 5.4; deposition time, 15 to 120 s.

Chemicals	Concentration ($g \cdot l^{-1}$)
$NiCl_2 \cdot 6H_2O$	15
$CH_3COOHNa \cdot 3H_2O$	10
NH_4Cl	50
$NaH_2PO_2 \cdot H_2O$	30
NF (48%)	$14\ ml \cdot l^{-1}$